Meccanica
https://doi.org/10.1007/s11012-024-01920-0

RESEARCH

Comparison between topological and surface sensitivities for shape optimization

Eric Segalerba · Emanuele Gallorini · Maurizio Quadrio · Jan Oscar Pralits

Received: 29 February 2024 / Accepted: 16 November 2024

Abstract The two most common shape-optimization methods for fluid mechanics problems are based on topology modifications and surface modifications. When the number of design parameters is large compared to the number of objective functions the most efficient way to evaluate the sensitivity derivatives is using the solution from adjoint equations. In external aerodynamics such as aircraft wings, cars, and trains, surface sensitivities are commonly applied since the topology remains the same and the surface quality and precision are important factors. In internal flows, such as ducts and tubes, the choice between topology and surface modifications is not trivial. Both methods can lead to useful optimal solutions, but either possesses its own pros and cons. Changing the topology might be admissible, and even adding material (duct thickness) can lead to unexpected topologically different solutions. This is also true in many bio-mechanical applications such as surgery of the upper airways (UA). In this paper, topological and surface sensitivities are evaluated and compared in OpenFOAM by solving the adjoint equations for a simple geometry first, and and then for the upper airways. Two different geometries of the UA are investigated: the first consists of only the nasal cavity and the sensitivity analysis is applied to the inner geometry and the surrounding walls. In the second case, a tissue of a certain thickness is added to the first to simulate a tissue removal around the existing airways. The different geometries are analyzed and discussed, evidencing also pros and cons of the different processes.

Keywords Bio fluid-dynamics · Adjoint equation method · Topological sensitivity · Shape sensitivity · Human nose

1 Introduction

In many fluid mechanics applications, the design boils down to optimising the shape of a certain geometry by minimising/maximising one or more metrics. Many optimization approaches exist and are usually divided into deterministic (gradient based), stochastic and robust methods [3]. Parametrisation of the geometry can also be made in different ways and we can divide the different approaches into two distinct categories: surface parametrisation and topological parametrisation. The first has a long history in aerodynamic shape

E. Segalerba (✉) · J. O. Pralits
Dipartimento di Ingegneria Civile, Chimica ed Ambientale, Università di Genova, Genova, Italy
e-mail: eric.segalerba@edu.unige.it

J. O. Pralits
e-mail: jan.pralits@unige.it

E. Gallorini · M. Quadrio
Dipartimento di Scienze e Tecnologie Aerospaziali, Politecnico di Milano, Milano, Italy
e-mail: emanuele.gallorini@polimi.it

M. Quadrio
e-mail: maurizio.quadrio@polimi.it

Published online: 04 December 2024

optimization [6, 8] while the second was developed for structural optimization [21]. Lately, also topological optimization has been extended to fluid dynamics applications [12]. This is for instance accomplished by adding a penalty field α proportional to the fluid velocity on the right-hand side of the momentum equations, the so-called Brinkman term [1]. When $\alpha \to \infty$ the velocity tends to zero and the corresponding computational cells behave as solids. A pure fluid domain is recovered when α is equal to zero. For intermediate values of α the fluid flows through a porous-like material. With this approach the topology of the domain can be changed, something that is impossible with a surface parametrisation. A disadvantage, however, with the topological approach is the imprecise definition of an interface, for instance, the surface between solid and fluid. The reason is that α is constant in the computational volume cells and does not follow a particular "sharp" interface which causes the interface itself to be tiered and its shape to be strongly dependent on cells size meaning that the smoothest surface, not aligned with the chosen coordinate system, will appear with a roughness given by the grid resolution, see Fig. 1. In particular, topological and surface parametrisation approaches are available in fluid dynamics applications using gradient-based methods [9]. The corresponding shape derivatives can be efficiently evaluated from the solution of adjoint equations [6, 11]. It is however not always straightforward to choose which method to use. In aeronautical applications such as the optimization of an airfoil, surface parametrisation is probably the best choice: only small changes in the geometry are allowed and the topology would be unchanged. What method should instead be used in biofluid dynamics applications is less obvious. Such problems range from surgery planning of the upper airways to facilitate breathing or enhance heat exchange, to stent design for vascular repair, etc. Moreover, in several applications, it might actually be enough to evaluate the sensitivities and then let the skilled end-user (eg. a surgeon or designer) make the decision based on the sensitivity results. In this paper the two approaches, topological and surface sensitivities, are evaluated, compared, and discussed. The sensitivities are computed by solving the adjoint equations. Existing methods, and corresponding theories, are briefly presented and discussed. Results from basic applications as well as the flow in the upper human airways are shown and discussed. The numerical solution of the flow equations is obtained using the open source finite volume solver OpenFOAM [20] and custom solvers for the adjoint field and the senstivities; the governing equations of the problem are the steady state, incompressible, isothermal Navier–Stokes equations. After a brief introduction, in Sect. 2 we describe the theory and

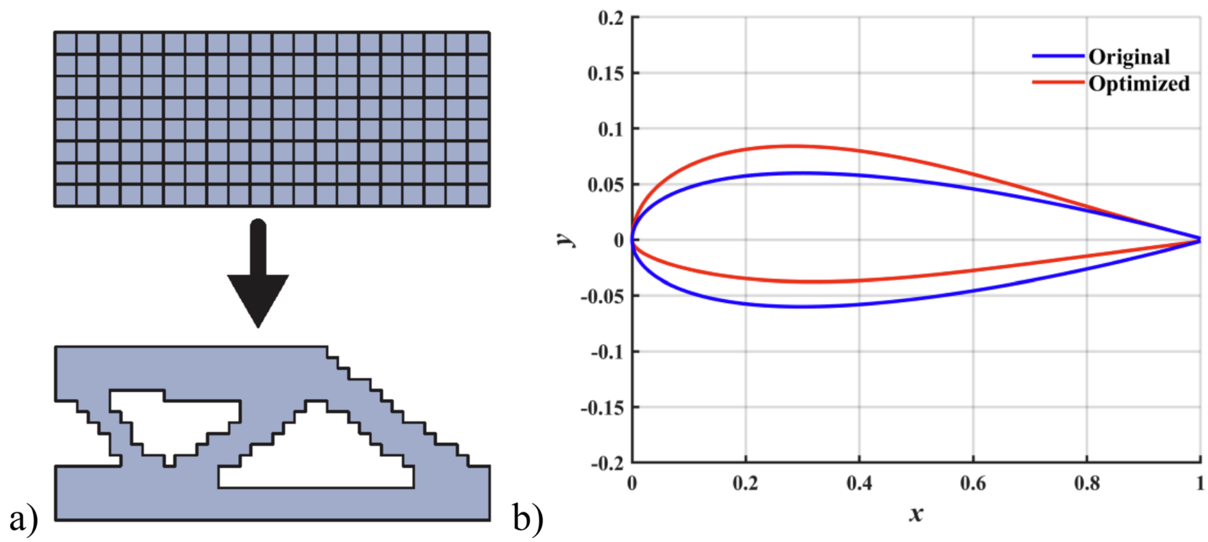

Fig. 1 **a** Topological approach: (top) grid resolution, (bottom) surface definition of an arbitrary shape. **b** deformations using surface sensitivities

numerical methods of the approaches studied. Results are presented for basic and applied cases in Sect. 3 followed by the conclusions.

2 Methods

The goal here is to compute and compare the sensitivity of a given objective function with respect to certain control variables using two different approaches: topological sensitivity and surface sensitivity, see [11]. The power, per unit mass, dissipated across the domain [10]

$$
\begin{aligned}
\mathcal{J}_{p_t} &= \int_{S_{I,O}} \left[-\left(p+\frac{1}{2}v_i^2\right)v_j\right]n_j dS = \\
&= \int_{S_O} \left[-\left(p+\frac{1}{2}v_i^2\right)v_j\right]n_j dS - \int_{S_I} \left[-\left(p+\frac{1}{2}v_i^2\right)v_j\right]n_j dS,
\end{aligned} \tag{1}
$$

is the objective function, being S_I and S_O the surfaces of the inlet and outlet sections. The sensitivities, i.e. gradients of the objective function with respect to the control variables, are evaluated from the solution of adjoint equations. Repeated indices, as in Eq. (1), imply summation from here on. We consider an incompressible flow where v_i are the velocity components and p is the pressure divided by the constant density, respectively. The formulation briefly presented here follows that of Papadimitriou and Giannakoglou [11] which considers laminar flow. The reason is to make equations and expressions more concise and clear. The governing equations, in the residual form, for the two sensitivity formulations are almost identical apart from the *Brinkman penalization term*, used in the topological formulation, here indicated by *top* (which stands for "topological"):

$$
\begin{cases}
R^p &= -\dfrac{\partial v_j}{\partial x_j}, \\
R_i^v &= v_j \dfrac{\partial v_i}{\partial x_j} - \dfrac{\partial \tau_{ij}}{\partial x_j} + \dfrac{\partial p}{\partial x_i} + \underbrace{\alpha\left(b_n\right)v_j}_{\text{top}}, \quad i = 1,2,3
\end{cases} \tag{2}
$$

where $\tau_{ij} = \nu\left(\frac{\partial v_i}{\partial x_j} + \frac{\partial v_j}{\partial x_i}\right)$ is the viscous stress tensor and ν being the effective viscosity. The term *"top"*, in Eq. 2, is governed by the porosity $\alpha\left(b_n\right)$. We assume an optimization problem expressed by the objective function $\mathcal{J}$ to be minimized, controlled by the variables $b_n (n = 1, ..., N)$ and constrained by the state equations $R_i = 0 (i = 1, ..., E)$, with E being the number of equations. The problem can be recast as an augmented objective function (or Lagrangian) $\mathcal{L}$, for which all variables are considered independent. The formulation of the Lagrangian includes an additional term which, for clarity, is written as an additional integral and not included in residuals and adjoint variables vectors. This constraint, whose details will be explained in the following, allows an easier evaluation of the gradients of the grid points with respect to the control variables, necessary to evaluate the Leibniz term [11] correctly. The Lagrangian is expressed as

$$
\mathcal{L} = \mathcal{J} + \int_V \Psi_i R_i dV + \int_V m_i^a R_i^m dV, \tag{3}
$$

where $\Psi_i (i = 1, ..., E)$ are the adjoint variables. Eq. (3) imposes constraints on the grid displacement m_i which is performed by using a Laplacian to diffuse the grid points, as shown in Eq. (4)

$$
R_i^m = \frac{\partial^2 m_i}{\partial x_j^2}. \qquad m_i = m_i\left(x_k, b_n\right). \tag{4}
$$

m_i^a is the adjoint variable associated to m_i. This governing equation, in the residuals form, is the Laplacian of m_i, which is the Cartesian displacement of the grid nodes, with respect to grid points. m_k is a function both of x_k and b_n since, respectively, this additional governing equation is satisfied on the given grid and the design variables directly affect its boundary conditions. The last constraint has been introduced to avoid computing the gradient of nodal displacements with respect to the control variables, in the whole domain [11].

We now seek stationary solutions of Eq. (3) by considering the first variation of $\mathcal{L}$, with respect to each variable, equal to zero [4, 11]. From the derivative with respect to the adjoint variables we obtain the governing equations for the fluid flow, Eq. (2), and grid displacements, Eq. (4). The derivative with respect to the control variable can now be written

$$
\frac{d\mathcal{L}}{db_n} = \frac{d\mathcal{J}}{db_n} + \frac{d}{db_n}\int_V \Psi_i R_i dV + \frac{d}{db_n}\int_V m_i^a R_i^m dV. \tag{5}
$$

The variables in Eq. (5) from the governing equations are factored out using repeated integration by parts. Moreover, the Leibnitz theorem and the Green-Gauss theorem are used to expand the resulting terms. A single adjoint equation, see Gallorini et al. [4] for a complete derivation, is written for the two sensitivity cases.

$$\begin{cases} R^q = -\dfrac{\partial u_j}{\partial x_j} + \left.\dfrac{\partial \mathcal{J}}{\partial p}\right|_V \\ R_i^u = u_j \dfrac{\partial v_i}{\partial x_j} - \dfrac{\partial\left(u_i v_j\right)}{\partial x_j} - \dfrac{\partial \tau_{ij}^a}{\partial x_j} + \dfrac{\partial q}{\partial x_i} + \underbrace{\alpha u_j}_{\text{adj-top}} + \left.\dfrac{\partial \mathcal{J}}{\partial u_j}\right|_V, \qquad i = 1,2,3 \end{cases} \tag{6}$$

where $\tau_{ij}^a = \nu\left(\frac{\partial u_i}{\partial x_j} + \frac{\partial u_j}{\partial x_i}\right)$. The only difference is the value of the Brinkman term, here denoted *adj-top*: for the case of surface sensitivity $\alpha(\mathbf{x}) = 0$. Moreover, the adjoint of the grid displacement PDE is given as

$$R_k^{m^a} = \frac{\partial^2 m_k^a}{\partial x_j^2} + \frac{\partial}{\partial x_j}\left\{ u_i v_j \frac{\partial v_i}{\partial x_j} + u_j \frac{\partial p}{\partial x_k} + \tau_{ij}^a \frac{\partial v_i}{\partial x_k} - u_i \frac{\partial \tau_{ij}}{\partial x_k} - q \frac{\partial v_j}{\partial x_k} \right\}, \tag{7}$$

where the right-hand side is given by the volume representation of the terms from the Leibnitz theorem. For a detailed analysis of the adjoint boundary conditions see Papadimitriou and Giannakoglou [11]. Fig. 2 illustrates graphically the two approaches to compute the sensitivity: panel *a*) presents the surface sensitivity approach, where the design variable b_n is a vector containing the coordinates of each surface node. The sensitivity with respect to the surface is computed as a function of the node coordinates and the actual displacement is proportional to the resulting gradient vector; in panel *b*) the topology is introduced through α, Brinkman's penalization term, which is included as a source term in the momentum equations, proportional to the velocity. Since α can be arbitrarily large a design variable $b_n = \eta$ is introduced, where $0 \leq \eta \leq 1$, and $\alpha = \alpha(\eta)$.

The surface derivative [7] of the objective function with respect to the control variables can now be written as

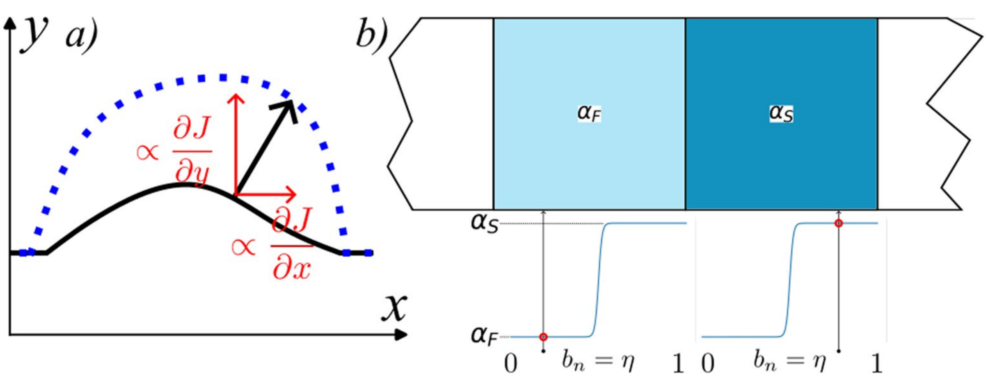

Fig. 2 Sketch of the two approaches to evaluate sensitivity. **a** presents the surface sensitivity approach where the design variable b_n is a vector containing the coordinates of each surface node. **b**the topology is introduced through α, which is is a source term in the momentum equations, proportional to the velocity

$$
\begin{aligned}
\frac{d\mathcal{J}}{db_n} = & -\int_{S_W} \left(\tau_{ij}^a n_j - q n_i + \frac{\partial \mathcal{J}_{S_W,l}}{\partial v_i} n_l\right) \frac{\partial v_i}{\partial x_k} \frac{dx_k}{db_n} dS - \int_{S_W} \frac{\partial m_i^a}{\partial x_j} n_j \frac{dx_i}{db_n} dS + \\
& + \int_{S_W} \frac{\partial \mathcal{J}_{S_W,i}}{\partial x_k} n_i \frac{dx_k}{db_n} dS + \int_{S_W} \mathcal{J}_{S_W,i} \frac{d\left(n_i dS\right)}{db_n} + \\
& - \int_{S_W} \left[\left(-u_k n_k + \frac{\partial \mathcal{J}_{S_W,k}}{\partial \tau_{lz} n_k n_l n_z}\right)\left(\tau_{ij} \frac{d\left(n_i n_j\right)}{db_n} + \frac{\partial \tau_{ij}}{\partial x_k} \frac{dx_k}{db_n} n_i n_j\right)\right] dS + \\
& - \int_{S_W} \left[\frac{\partial \mathcal{J}_{S_W,k}}{\partial \tau_{lz}} n_k t_l^I t_z^I \left(\tau_{ij} \frac{d\left(t_i^I t_j^I\right)}{db_n} + \frac{\partial \tau_{ij}}{\partial x_k} \frac{dx_k}{db_n} t_i^I t_j^I\right)\right] dS + \\
& - \int_{S_W} \left[\left(\frac{\partial \mathcal{J}_{S_W,k}}{\partial \tau_{lz}} n_k \left(t_l^{II} t_z^I + t_k^I t_z^{II}\right)\right)\left(\tau_{ij} \frac{d\left(t_i^{II} t_j^I\right)}{db_n} + \frac{\partial \tau_{ij}}{\partial x_k} \frac{dx_k}{db_n} t_i^{II} t_j^I\right)\right] dS + \\
& - \int_{S_W} \left[\frac{\partial \mathcal{J}_{S_W,k}}{\partial \tau_{lz}} n_k t_l^{II} t_z^{II} \left(\tau_{ij} \frac{d\left(t_i^{II} t_j^{II}\right)}{db_n} + \frac{\partial \tau_{ij}}{\partial x_k} \frac{dx_k}{db_n} t_i^{II} t_j^{II}\right)\right] dS,
\end{aligned}
\tag{8}
$$

where t_i^I and t_i^{II} are the two components of the unit vectors tangent to the surface and S_W is the wall boundary.

The sensitivity with respect to a topological change (sometimes denoted "solidification" of volume's cells) [4] is simply given by

$$
\frac{d\mathcal{J}}{db_n} = \int_V u_i v_j \frac{\partial \alpha}{\partial b_n} dV, \tag{9}
$$

A significant difference between the topological and surface formulations is how the surface of a certain geometry is defined. In the surface formulation, a solid surface is defined by the initial geometry and corresponding boundary conditions (non-slip, impermeable, adiabatic,...), and the smoothness (continuous curvature) is usually maintained during the optimization. In topological optimization the formulation assumes that the geometry is represented by a certain density (or porosity). The lower the porosity, the less fluid will penetrate. In the limit of zero porosity the geometry will behave as an impermeable solid and zero velocity will be implicitly defined on its borders (surface). When the porosity varies gradually from large to small, there is no clear limit/border where to define a solid surface. In certain applications, this is an accepted result and it comes down to the designer to define a distinct surface between one material and another. This can however be made more rigorously by introducing certain "transition" functions. One such example is the sigmoid function [14] which allows for a sharp transition from low to high permeability and this can be achieved by introducing a new control variable η which varies from 0 to 1:

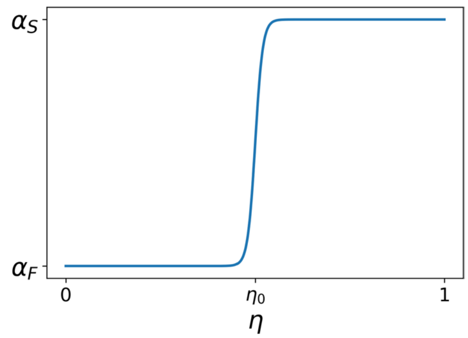

Fig. 3 α as a function of η

$$
\alpha = \alpha(\eta) = \alpha_S + \left(\alpha_F - \alpha_S\right) \frac{1}{1 + e^{-k(\eta - \eta_0)}}. \tag{10}
$$

In Eq. (10) α_S and α_F are the upper and lower limit values of α, respectively. A value of η between 0 and the threshold, defined by the user, η_0 defines the fluid domain while values between η_0 and 1 denotes a solid; the threshold η_0 controls around which value of η the transition should take place.

Finally, the transition interval can be controlled by the value of the parameter k: the larger the value of k, the faster the transition from α_F to α_S. An example is given in Fig. 3.

3 Results

3.1 Numerical implementation

The numerical results presented here are obtained from solutions computed with the open-source software OpenFOAM [20], version 10. At the present time no OpenFOAM version has both topological and surface sensitivity approaches implemented. We therefore applied the adjoint-based topology approach implemented by Gallorini et al. [4, 5], and the adjoint-based surface sensitivity (E-SI) approach by Kavvadias et al. [7] as implemented in Pizzolato [13].

In all cases the finite-volume method is used and the solvers are second-order accurate. The turbulence model used is $k-\omega$ and the SIMPLE algorithm solves the direct and adjoint equations. Convergence is considered when the residuals reach an asymptotic value, always below 10^{-2}. The adjoint

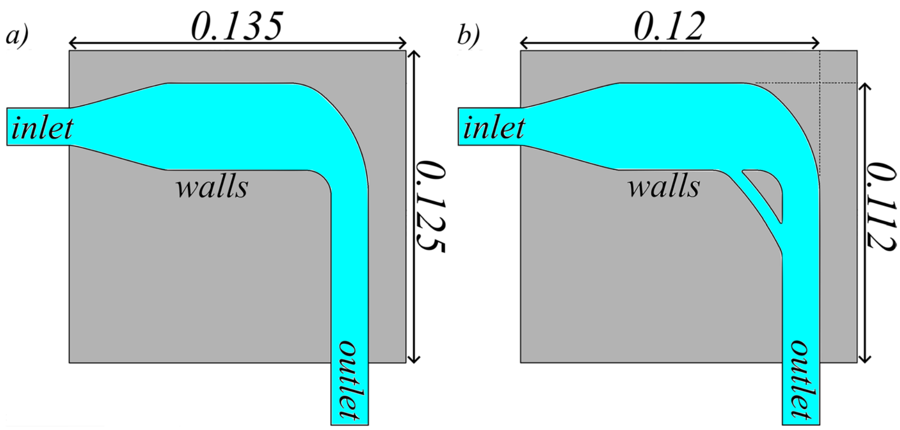

Fig. 4 Geometry and overall dimensions (in meters) of the two convergent/divergent elbow ducts: **a** single duct; **b** duct with bypass channel. Fluid domain (light blue), solid domain (gray) used in the topological sensitivity analysis. The two duct sections, close to inlet and outlet, outside the solid contour, are set to symmetry and do not contribute to flow development or sensitivity. (Color figure online)

equations used here are derived using the "frozen" turbulence approach. This means that the variation of the turbulent viscosity is assumed zero in the adjoint derivation.

3.2 Sensitivity comparison for two ducts

The sensitivity analyses are here applied to two bi-dimensional ducts, see Fig. 4, shaped as divergent/convergent elbows. The first is a single duct, while the second has an additional bypass channel. Since the additional bypass channel introduces a resistance, and a topological difference, it is considered a significant test case to observe the solution from the two sensitivities of the function defined in Eq. 1 The grey box surrounding the duct is active only in the topological approach where α is zero in the channel while high enough to act as a non-porous solid in the grey region. This means that for each duct the fluid flows in identical geometries in both approaches. The difference might be seen in the sensitivity analysis where the topological approach could allow the sensitivity to extend also in the solid (grey) domain. In all calculations the volumetric flow rate $\dot{Q} = 2.667 \cdot 10^{-4}$ $[m^3/s]$ is imposed at the inlet with a zero-gradient condition for pressure. A constant static pressure of $p = 0$ $[Pa]$ and zero velocity gradient is applied at the outlet. In all the cases a background mesh of hexahedral cells with dimension $1 \cdot 10^{-3}$ $[m]$ is adopted and a two-level refinement on the *walls*, *inlet* and *outlet* is applied to have a characteristic length of $2.5 \cdot 10^{-4}$ $[m]$. In the surface sensitivity case, 6 inflation layers are added on the *wall* boundaries. Both meshes have non-orthogonality lower than 60° and maximum skewness below 4.

In Fig. 5 the results of surface and topological sensitivities are presented as vectors normal to the surface, and contours, respectively. The two sensitivity analyses indicate similar modifications to the geometry: the inlet should be widened, and so should the inner elbow corner and the straight vertical channel towards the outlet. Some differences can be noticed: a modification of the outer elbow surface is present only in the topological case. A sign difference appears in the topological sensitivity in the wall-normal direction of the inner elbow surface. Such a result is not obtainable in the surface case since the sensitivity is evaluated only along the boundary. Moreover, a shape deformation according to the surface sensitivities would result in a smooth surface, while the topologically reshaped geometry will be rougher due to the solid-void transition.

Figure 6 presents the results for the duct with an additional small bypass channel in the inner elbow corner. As can be noticed from the sensitivity maps, the main differences are located in the solid region between the bypass channel and the main one: in the topological sensitivity the red area indicates where the solid should be re-inforced while the blue strip along the surface should be removed; in between

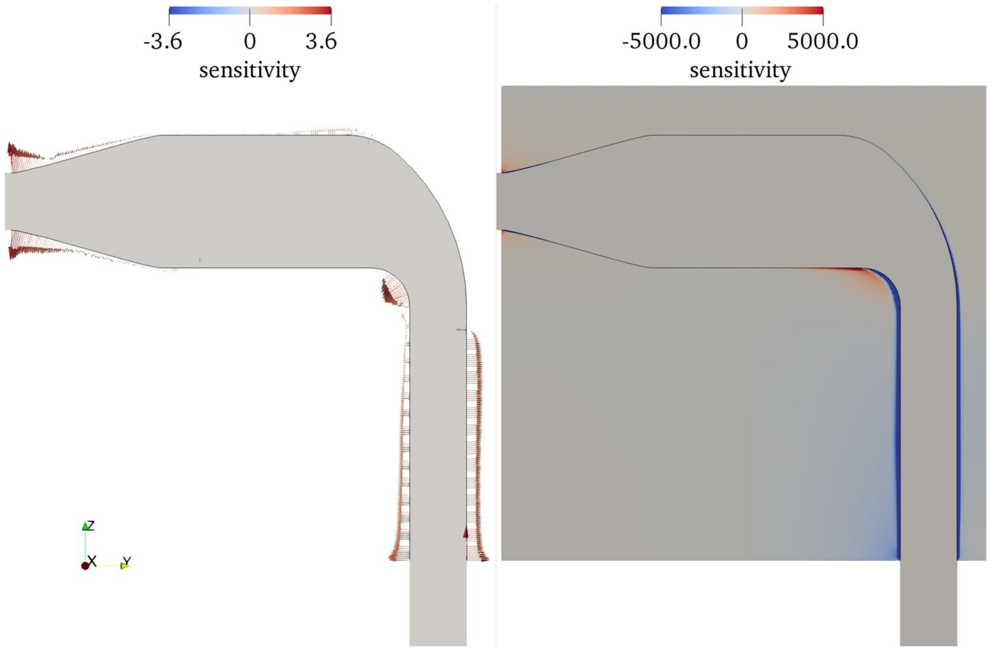

Fig. 5 Surface (left) and topological (right) sensitivities for the simple duct geometry. The surface sensitivity is shown as vectors whose direction is normal to the surface, while the magnitude is proportional to the gradient value. For the topological sensitivities negative gradients (color blue) indicate counterproductive cells (to be removed) while positive gradients (color red) indicate productive cells (material to be added). (Color figure online)

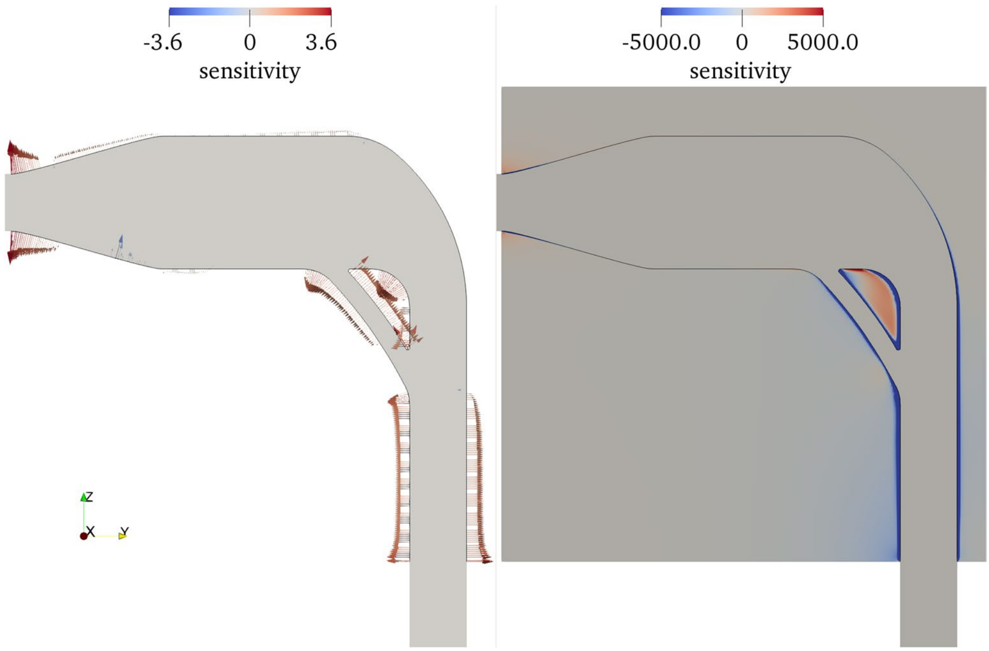

Fig. 6 Surface (left) and topological (right) sensitivities for the duct with the bypass channel. Color schemes and legends as in Fig. 5. (Color figure online)

there is a thin line where the new geometry will be defined. In the case of surface sensitivity, the results indicate that the hollow gap should be decreased but it is less evident in what way. In the limit of large deformations, a thin strip of material will be left, since the topology cannot change.

3.3 Sensitivity comparison for the flow in the upper airways

The surface and topology-based approaches are compared for the flow in the upper airways. The geometry considered in this work is obtained from the STL file of Saibene et al. [17] in which a CT scan, segmented at constant radiodensity threshold, is reconstructed under the supervision of an ENT expert, according to a previously described procedure [15]. The choice of using such a geometry is determined mainly by two reasons: first, the geometry of the upper airways is very complex (containing convergent, divergent, and narrow sections, high curvature, and surfaces with different roughness); these properties make it a severe test, able to show the strength and weaknesses of the approaches. The second reason is that breathing difficulties are widespread and usually difficult to diagnose [16, 18]; clinicians face the issue of understanding if the deformities detected in the medical examination are the cause of patient's symptoms and many times the answer is not straightforward. Surgeons make assumptions based on their experience, and errors are unavoidable [19]: this promotes the search for an objective tool to help them during the decision phase, and sensitivity analysis is a promising method.

The resulting three-dimensional geometry, augmented by a spherical air volume surrounding the external nose [2], is shown in Fig. 7a. The latter moves the inlet portion of the computational domain far from the nostrils, minimizing the computational overhead. The full potential of topological sensitivity can only be exploited if a solid surrounding the fluid volume is included. In the case of the upper airways, this means adding the surrounding tissue. We model this by adding a "Surgery box" of tissue around a part of the geometry shown in Fig. 7a. The resulting geometry is presented in Fig. 7b.

From a surgical point of view adding material is not standard practice nor feasable but the algorithm, at this stage, is not tailored for this specific case where material can only be removed. It should be noticed tough that the regions where material is added are few so the sensitivity gives useful insights. The

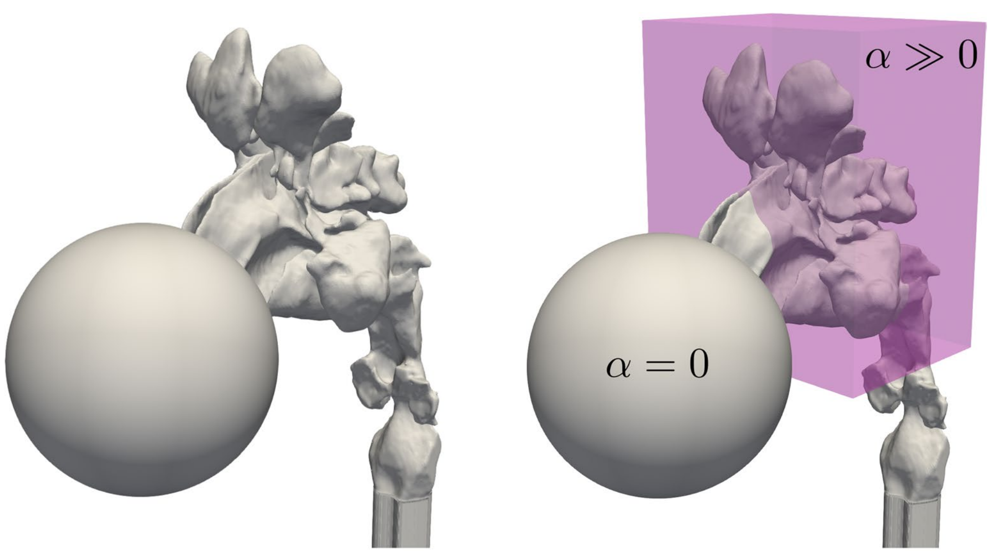

(a) standard geometry

(b) geometry with "surgery box"

Fig. 7 Geometries of the upper airways used for the two sensitivity formulations. **a** shows the fluid domain; **b** shows the configuration in (**a**) with an additional surgery box (the part with lower opacity) used only in the case of topological sensitivity. In the surgery box, a high value of α is assigned to model a solid meshes have max non-orthogonality lower than 65°, max skewness lower than 4, and there are no inflation layers. Dimensions are similar to the simple ducts shown previously, with a height of 0.16 [m] a depth of 0.14 [m] (in the sagittal plane), and a width of 0.08 [m] (in the coronal plane).

A constant volumetric flow rate of $\dot{Q} = 2.667 \cdot 10^{-4}$ [m^3/s] ~ 16 [l/m] is applied at the external boundary along with a zero gradient condition for the pressure. At the outlet (throat), a zero gradient condition for the velocity $\partial u_i/\partial n = 0$ is applied, while the pressure is set to a reference value of 0. At the walls, which are the inner parts of the nose, a no-slip boundary condition holds; the flow is transitional but, to simplify calculations, it is made the approxiamtion of fully turbulent flow and the turbulence is modeled using a standard $k - \omega$ SST model. This setup guarantees physiological flow conditions for a human at rest without breathing pathologies. The boundary conditions applied to the adjoint equations, in the topological case for velocity and pressure at the inlet, are:

$$\begin{cases} v_n = -\dfrac{\partial \mathcal{J}}{\partial p} \\ \mathbf{v}_t = 0 \\ (\mathbf{n} \cdot \nabla) q = 0. \end{cases}$$

At the outlet, the boundary conditions are:

$$\begin{cases} q = \mathbf{u} \cdot \mathbf{v} + u_n v_n + \nu (\mathbf{n} \cdot \nabla) v_n + \dfrac{\partial \mathcal{J}}{\partial u_n} \\ u_n \mathbf{v}_t + \nu (\mathbf{n} \cdot \nabla) \mathbf{v}_t = -\dfrac{\partial \mathcal{J}}{\partial \mathbf{u}_t}. \end{cases}$$

To couple the normal and the tangential components of the velocity, the following relation, obtained from the continuity, can be applied:

$$\nabla \cdot \mathbf{v} = (\mathbf{n} \cdot \nabla) v_n + \nabla_{||} \cdot \mathbf{v}_t = 0 \rightarrow (\mathbf{n} \cdot \nabla) v_n = -\nabla_{||} \cdot \mathbf{v}_t$$

The meshes presented in this work are constructed using *snappyHexMesh* and are mostly made up of hexahedral cells. The grid is around seven million cells, non-orthogonality is below 65°, and max skewness is below 4°. The numerical setup for the cases is standard practice for RANS equations with the quality of the elements.

The surface sensitivity, obtained using the E-SI formulation [7] on the standard nasal geometry, is presented in Fig. 8. It indicates how to modify the surface to minimize the power drop across the domain.

It can be noticed, especially from the bottom view, that there are sensitivity oscillations related to the

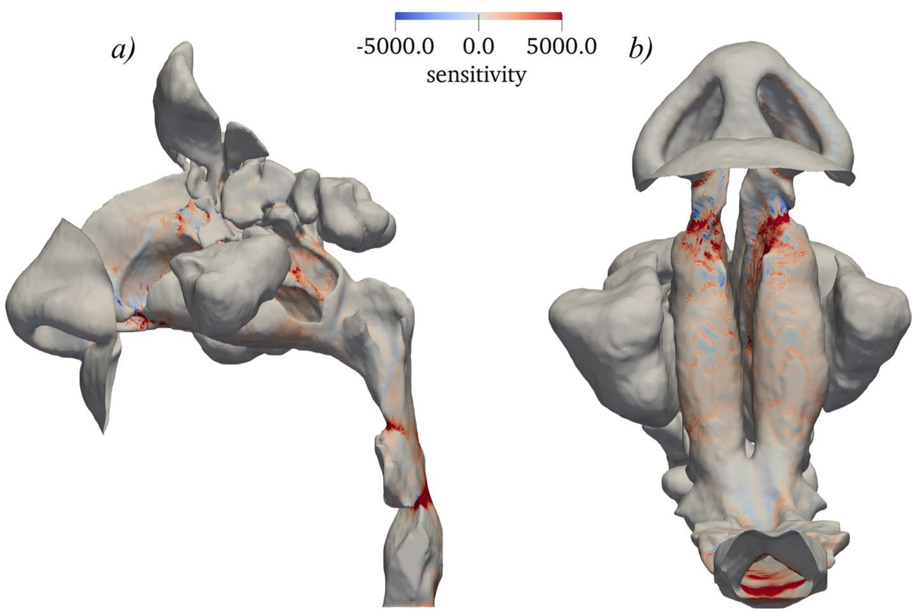

Fig. 8 Surface sensitivity. The *red* stands for push out while *blue* means pull in. **a** is the sagittal view, **b** the bottom view. (Color figure online)

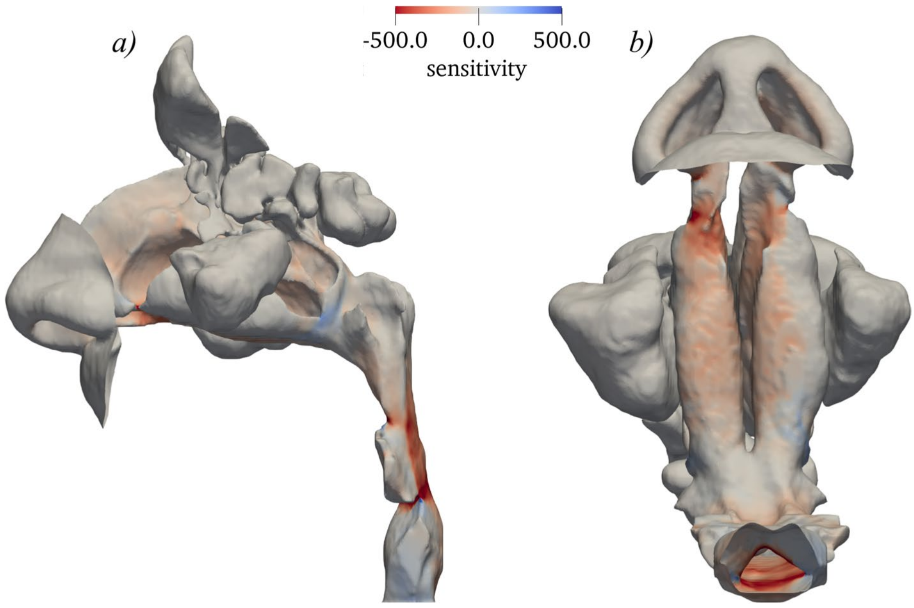

Fig. 9 Topological sensitivity. The *red* means to add material while *blue* means to remove. **a** is the sagittal view, **b** the bottom view. (Color figure online)

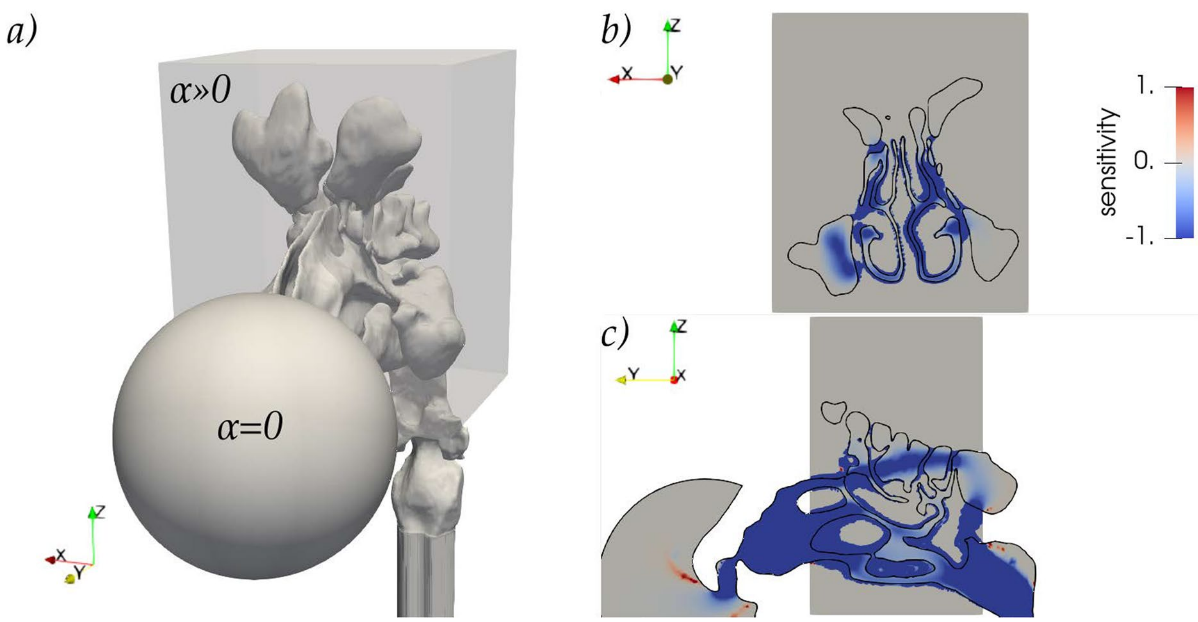

Fig. 10 Topological sensitivity evaluated on the upper airways including a model of the surrounding tissue ("Surgery box"); **a** coronal view; **b** para-sagittal plane through the left nostril. The fluid and solid domains are light gray and black, respectively. The shadowed gray contour represents the region where solid material should be removed. (Color figure online)

roughness of the nasal surface: to reduce the power drop the sensitivity aims to flatten (smooth) the surface.

Figure 9 shows the results of the topological sensitivity evaluated on the surface of the standard geometry of the nose.

In general, topological optimization is performed by assigning a momentum loss to cells that negatively impact the cost function. In this case, *blue* cells are counterproductive (to be removed), while *red* cells are productive (to remain or be added). It can be noticed that there are fewer oscillations compared to the previous case. This can be related to the lower influence of the surface shape since the gradient is evaluated in the whole cell rather than the faces. Apart from some small differences, such as wall roughness, the two sensitivity approaches, evaluated on the surface of the nose cavity, provide similar indications.

The absence of a region from which to remove material limits the potential of topological sensitivity, so an external box called "Surgery Box" is added, see Fig. 10. Porosity α controls the transition from void to solid: in the fluid, its value is 0, while in the box, it is high to cause a large momentum loss mimicking the characteristics of a solid. Figures 10a and b present the results for a coronal and sagittal plane. An intuitive solution to decrease the objective function exploited here is to increase the cross-section of the different cavities. This would be straightforward using surface sensitivities. Here instead, with the addition of the surrounding tissue, we obtain indications of what to modify also in the solid region. Clearly, in some parts, the sensitivity suggests increasing the cross-section of the air, like in the lower parts of the nasal cavity, see Fig. 10b. However, some topological changes are visible in the results presented in the coronal plane where some cavities are connected. Such changes could be interpreted as tissue being removed during surgery and only possible by modeling also the surrounding tissue.

4 Conclusions

Two adjoint-based sensitivity analyses are compared, namely topology and surface (or shape) sensitivities, to understand when one performs better than the other, scrutinizing their differences. Both approaches are evaluated numerically using OpenFOAM 10, with the sensitivity routines implemented according to previously published investigations. The power per unit mass is used as the objective function, and different geometries are studied: two simple elbow ducts and a three-dimensional geometry of the upper airways reconstructed from a CT scan of an adult person.

It is shown that surface sensitivities work well when the geometrical description must be accurate, and no post-processing of the final geometry is necessary. However, topological changes can not be accounted for, and they amplify existing irregularities in the geometry surface. The latter is not easily overcome in an optimization loop since the gradient update is linear and the amplitude of the geometrical modification is arbitrary. This behavior was visible in the application of the upper airways. Topological sensitivities are favorable when topology changes of an initial geometry are admissible and few geometrical constraints are used. Moreover, since the sensitivities are also evaluated in the solid region, both a decrease and an increase in the fluid volume are possible. Compared to surface sensitivities, irregularities of the initial geometry are less visible since its values are constant in the finite-volume cell, averaging out local variations. With topology sensitivity, a scalar value determines the geometry (void, porous, or solid) in each finite-volume cell: a sharp description of the fluid-solid interface is therefore impossible. Without countermeasures, a transition between void and solid will appear where a variable porosity will substitute the sharp interface. There are some techniques to render this transition, more or less, sharp. This paper illustrates one based on a sigmoid function. In applications such as surgery of the upper airways, the approach based on topology sensitivities is favorable if the surrounding tissue is modeled. In this way, surgery by removing tissue and modifying the topology is possible, as in the virtual surgery shown in Saibene et al. [17].

Acknowledgements We express our sincere gratitude to the OpenFOAM Workshop 18 organizing committee for their invaluable support.

Author contributions Eric Segalerba and Jan Pralits wrote the main manuscript. Emanuele Gallorini and Maurizio Quadrio wrote the numerical solvers used in this work. All the authors took part in the review process.

Funding The authors did not receive support from any organization for the submitted work.

Ddata availability At the moment no open dataset used is available.

Declarations

Conflict of interest The authors declare no conflict of interest.

Ethical Approval Not applicable.

References

1. Angot P, Bruneau CH, Fabrie P (1999) A penalization method to take into account obstacles in incompressible viscous flows. Numerische Math 81:497–520
2. Balatinec L, Uroić T, Jasak H (2021) Open-source cfd analysis of nasal flows. 1: 2–26. https://doi.org/10.51560/ofj.v1.38
3. Cavazzuti M (2013) Optimization methods: from theory to design. Springer, Berlin Heidelberg
4. Gallorini E, Hèlie J, Piscaglia F (2023) An adjoint-based solver with adaptive mesh refinement for efficient design of coupled thermal-fluid systems. Int J Numer Methods Fluids 95(7):1090–1116. https://doi.org/10.1002/fld.5179
5. Gallorini E, Hèlie J, Piscaglia F (2023) A multi region adjoint-based solver for topology optimization in conjugate heat transfer problems. Comput & Fluids 266:106042. https://doi.org/10.1016/j.compfluid.2023.106042
6. Jameson A, Martinelli L (2000) Aerodynamic shape optimization techniques based on control theory, pp. 151–221. Berlin, Heidelberg: Springer Berlin Heidelberg
7. Kavvadias I, Papoutsis-Kiachagias E, Giannakoglou K (2015) On the proper treatment of grid sensitivities in continuous adjoint methods for shape optimization. J Comput Phys 301:1–18. https://doi.org/10.1016/j.jcp.2015.08.012
8. Martins JR (2022) Aerodynamic design optimization: challenges and perspectives. Comput & Fluids 239:105391. https://doi.org/10.1016/j.compfluid.2022.105391
9. Othmer C (2008) A continuous adjoint formulation for the computation of topological and surface sensitivities of ducted flows. Int J Numer Methods Fluids 58(8):861–877. https://doi.org/10.1002/fld.1770
10. Othmer C, de Villiers E, Weller H (2007) Implementation of a continuous adjoint for topology optimization of ducted flows. AIAA Paper 2007–3947
11. Papadimitriou DI, Giannakoglou KC (2008) Direct, adjoint and mixed approaches for the computation of hessian in airfoil design problems. Int J Numer Methods Fluids 56(10):1929–1943. https://doi.org/10.1002/fld.1584
12. Papoutsis-Kiachagias E, Giannakoglou K (2014) Continuous adjoint methods for turbulent flows, applied to shape and topology optimization: industrial applications. Arch Comput Methods Eng 23:255–299
13. Pizzolato F (2023) Thermal-adjoint solver for multi-objective shape optimisation based on continuous adjoint method
14. Popovac M (2022) Continuous adjoint topology optimization of duct flow configurations with explicit volume constraint for design variable update. Energies 15:7349
15. Quadrio M, Pipolo C, Corti S, Messina F, Pesci C, Saibene A, Zampini S, Felisati G (2016) Effects of ct resolution and radiodensity threshold on the cfd evaluation of nasal airflow. Med & Biol Eng & Comput 54(2–3):411–9. https://doi.org/10.1007/s11517-015-1325-4
16. Rudmik L, Soler ZM, Mace JC, Schlosser RJ, Smith TL (2015) Economic evaluation of endoscopic sinus surgery versus continued medical therapy for refractory chronic rhinosinusitis. The Laryngoscope 125(1):25–32. https://doi.org/10.1002/lary.24916
17. Saibene A, Felisati G, Pipolo C, Bulfamante A, Quadrio M, Covello V (2020) Partial preservation of the inferior turbinate in endoscopic medial maxillectomy: a computational fluid dynamics study. Am J Rhinol & Allergy 34(3):409–416. https://doi.org/10.1177/1945892420902005
18. Smith K, Orlandi R, Rudmik L (2015) Cost of adult chronic rhinosinusitis: a systematic review. The Laryngoscope 125:1547–1556. https://doi.org/10.1002/lary.25180
19. Sundh C, Sunnergren O (2015) Long-term symptom relief after septoplasty. Eur Arch Otorhinolaryngol 272(10):2871–2875. https://doi.org/10.1007/s00405-014-3406-7
20. Weller HG, Tabor G, Jasak H, Fureby C (1998) A tensorial approach to computational continuum mechanics using object-oriented techniques. Comput Phys 12(6):620–631. https://doi.org/10.1063/1.168744
21. Wu J, Sigmund O, Groen J (2021) Topology optimization of multi-scale structures: a review. Struct Multidisc Optim 63:1455–1480. https://doi.org/10.1007/s00158-021-02881-8